Chen, Guangze; Lado, Jose

Impurity-induced resonant spinon zero modes in Dirac quantum spin liquids

Impurity-induced resonant spinon zero modes in Dirac quantum spin liquids

Guangze Chen ⊙ and J. L. Lado ⊙
Department of Applied Physics, Aalto University, 02150 Espoo, Finland

Quantum spin liquids are strongly correlated phases of matter displaying a highly entangled ground state. Because of their unconventional nature, finding experimental signatures of these states has proven to be a remarkable challenge. Here we show that the effects of local impurities can provide strong signatures of a Dirac quantum spin-liquid state. Focusing on a gapless Dirac quantum spin-liquid state as realized in $NaYbO_2$, we show that a single magnetic impurity coupled to the quantum spin-liquid state creates a resonant spinon peak at zero frequency, coexisting with the original Dirac spinons. We explore the spatial dependence of this zero-bias resonance and show how different zero modes stemming from several impurities interfere. We finally address how such spinon zero-mode resonances can be experimentally probed with inelastic spectroscopy and electrically driven paramagnetic resonance with scanning tunnel microscopy. Our results put forward impurity engineering as a means of identifying Dirac quantum spin liquids with scanning probe techniques, highlighting the dramatic impact of magnetic impurities in a macroscopically entangled many-body ground state.

I. INTRODUCTION

Quantum spin liquids (QSL) [1–3] are exotic magnetic phases of matter, characterized by strong quantum fluctuations and frustration [4], lacking magnetic order even at zero temperature [5]. The unique properties of quantum spin liquids have attracted much research interest [6–8], in particular for their emergent Majorana physics [9] and their long-standing relation with unconventional superconductivity [10,11]. A variety of compounds showing quantum spin-liquids physics have been identified [12–22], including the gapless triangular lattice Dirac quantum spin-liquid in $NaYbO_2$ [23,24] and different van der Waals materials [25–28]. Interestingly, finding gapless Dirac spin liquids in van der Waals materials would provide a spinon version of graphene Dirac electrons, opening the door to explore strain gauge fields in spinons [29–31], spinon flat bands by twist engineering [32–35], and impurity-induced spinon resonances [36,37].

Impurities have been recognized as a powerful indicator to identify exotic electronic orders [38]. A paradigmatic example of this is the nonmagnetic impurities in unconventional superconductors [39], where the emergence of in-gap states is a well-known signature of unconventional superconductivity [40–43]. In contrast, conventional *s*-wave superconductors do not show such in-gap states in the presence of nonmagnetic impurities [44], and only magnetic impurities can give rise to in-gap modes [45–47]. Impurities are also a simple way of imaging the Fermi surface of metals, by measuring Friedel oscillations with scanning probe techniques [48–50]. Other

paradigmatic examples are carbon vacancies [36,51–56] and hydrogen ad-atoms [57,58] in graphene, giving rise to a divergent density of states [36,52] and magnetism [37,53,58]. Along this line, recent experimental advances have demonstrated the possibility of single-atom manipulation in a variety of systems by means of scanning probe techniques [59–73]. This motivates the question of whether single-atom manipulation [74] can detect unique features of quantum spin-liquid states.

Here we show that, by depositing individual magnetic atoms on top of a Dirac quantum spin liquid, spinon resonances can be engineered. We demonstrate that the Dirac quantum spin-liquid ground state develops resonant zero modes, and we study the interference effects between these spinon zero modes. Finally, we show that divergent spinon density of states can be experimentally probed by means of inelastic spectroscopy and electrically driven paramagnetic resonance with scanning tunnel microscopy. Our results put atomically controlled defect engineering as a powerful local probe of Dirac quantum spin-liquid physics, opening up a simple technique to identify fractionalized quantum states of matter with real space measurements.

Our paper is organized as follows. In Sec. II, we show that single magnetic impurities create zero-energy resonances in a Dirac quantum spin liquid. In Sec. III, we study the interference effects between different spinon resonances. In Sec. IV, we elaborate how such spinon resonances can be probed by means of scanning tunneling spectroscopy techniques. Finally, in Sec. V, we summarize our conclusions.

II. SINGLE SPIN IMPURITY IN A DIRAC SPIN LIQUID

In this section, we show the emergence of resonant zero modes in presence of a single impurity in a gapless Dirac spin liquid. We consider two different limiting cases: (i) a periodic
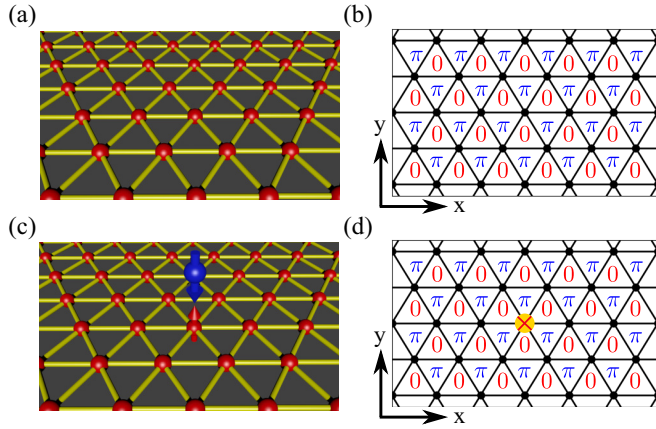
FIG. 1. (a) Sketch of a Dirac quantum spin-liquid state in the triangular lattice, together with (b) the effective mean-field spinon π-flux model. (c) Sketch of a magnetic moment coupled to the triangular Dirac quantum spin liquid. The magnetic impurity (blue) couples to the site underneath (red), creating a singlet state $|\uparrow\downarrow\rangle - |\downarrow\uparrow\rangle$ and removing the spin degree of freedom of the coupled site from the QSL. The combination of the magnetic impurity with the mean-field partonic transformation of Eq. (2) gives rise to an effective model featuring a π-flux lattice with a vacant site (d).

array of impurities with each impurity in a unit cell of size $n \times m$ and (ii) a single impurity in an infinitely large system.

The spinon excitations in triangular spin liquids [Fig. 1(a)] such as $NaYbO_2$ are captured by the π-flux model on the triangular lattice [Fig. 1(b)]. The elementary excitations of the π-flux state are Dirac fermions at half-filling. A local $S = 1/2$ magnetic moment coupled to the quantum spin-liquid state [Fig. 1(c)] gives rise to a vacancy in the effective spinon model [Fig. 1(d)]. As we will see below, the existence of the magnetic impurity creates a divergent density of states in the spinon spectra. For the sake of completeness, we first introduce the spinon properties of the pristine quantum spin liquid, and we then move to study the effect of a magnetic impurity.

A. Spinon excitations in a pristine Dirac spin liquid

We start by taking a quantum spin model in a triangular lattice with the general form

$$\mathcal{H} = \sum_{ij} J_{ij}^{\mu\nu} S_i^\mu S_j^\nu, \qquad (1)$$

where $J_{ij}^{\mu\nu}$ are exchange constants between sites i, j for the spin components μ, ν, and S_i^μ is the μ component of the spin operator for the site i. The previous Hamiltonian describes a purely many-body system, whose exact solution cannot be generically found analytically. The previous model on a triangular lattice is known to give rise to a quantum spin-liquid state, when one considers first and second neighbor interactions [75–77]. An approximate solution in a quantum spin-liquid state can be obtained by performing the parton transformation [8]

$$\mathbf{S} = \frac{1}{2} f_\alpha^\dagger \sigma_{\alpha\beta} f_\beta \qquad (2)$$

to the model Eq. (1). The parton transformation separates the frozen charge degree of freedom and the free spin degree of freedom in the quantum spin-liquid state, with $f_\alpha^\dagger$ and f_α being fermionic spinon operators with spin-1/2 α satisfying $\sum_\alpha f_\alpha^\dagger f_\alpha = 1$. At the partonic mean-field level, and upon the appropriate regime in the exchange couplings [76], the above spin Hamiltonian gives rise to the π-flux state [75,78] [Fig. 1(b)]:

$$H = t \sum_{\langle i,j \rangle} \chi_{ij} f_i^\dagger f_j, \qquad (3)$$

where $\chi_{ij} = \pm 1$ and t are mean-field parameters. The π-flux state hosts alternating $0, \pi$ fluxes per unit cell. The elementary excitations of the π-flux Hamiltonian are spinon Dirac fermions. In the following, we show how the presence of a magnetic impurity modifies the previous picture.

B. Spinon resonances with periodic impurities

We now move on to consider the effect of magnetic impurities coupled to the Dirac quantum spin-liquid state. The total Hamiltonian of the system is

$$\mathcal{H} = \mathcal{J} \sum_{k \in \mathcal{K}} \mathbf{s}_k \cdot \mathbf{S}_k + \sum_{ij} J_{ij}^{\mu\nu} S_i^\mu S_j^\nu, \qquad (4)$$

where $\mathbf{s}_k$ are the spin operators for the different $S = 1/2$ ad-atoms considered, $\mathcal{K}$ denotes the sites that have an impurity ad-atom on top, and $\mathcal{J}$ is the antiferromagnetic exchange coupling between the magnetic ad-atom and the site below. Taking the limit of strongly coupled magnetic impurity $\mathcal{J} \gg J_{ij}^{\mu\nu}$, the different sites k will form a singlet state with the impurity on top, effectively removing the $S = 1/2$ from the quantum spin-liquid compound. As a result, the effective Hamiltonian in this limit is

$$\mathcal{H} = \sum_{ij, i \notin \mathcal{K}, j \notin \mathcal{K}} J_{ij}^{\mu\nu} S_i^\mu S_j^\nu, \qquad (5)$$

an effective triangular model where the sites hosting a magnetic impurity above disappear from the low-energy Hamiltonian. Using an analogous spinon replacement as before, we obtain that the effective model for the spinons becomes

$$H = t \sum_{\langle i,j \rangle, i \notin \mathcal{K}, j \notin \mathcal{K}} \chi_{ij} f_i^\dagger f_j, \qquad (6)$$

an effective π-flux model with impurities determined by the magnetic ad-atoms deposited. (We here approximate that the mean-field spinon model does not have nontrivial reconstructions.) As a result, a magnetic impurity becomes equivalent to a vacancy in the effective spinon model. We note that this equivalence holds only for $S = 1/2$ impurities, as higher S impurities would generate a free degree of freedom in each site even in the limit $\mathcal{J} \gg J_{ij}^{\mu\nu}$. We also note that given that the magnetic ad-atoms on top can be moved with a scanning tunnel microscope [59–73], this would allow us to engineer models with an arbitrary number of vacancies in the effective spinon model.

We now explore the spectra of this defective quantum spin-liquid state. When considering a periodic array of impurities in unit cells of size $n \times m$, the Bloch Hamiltonian can be used
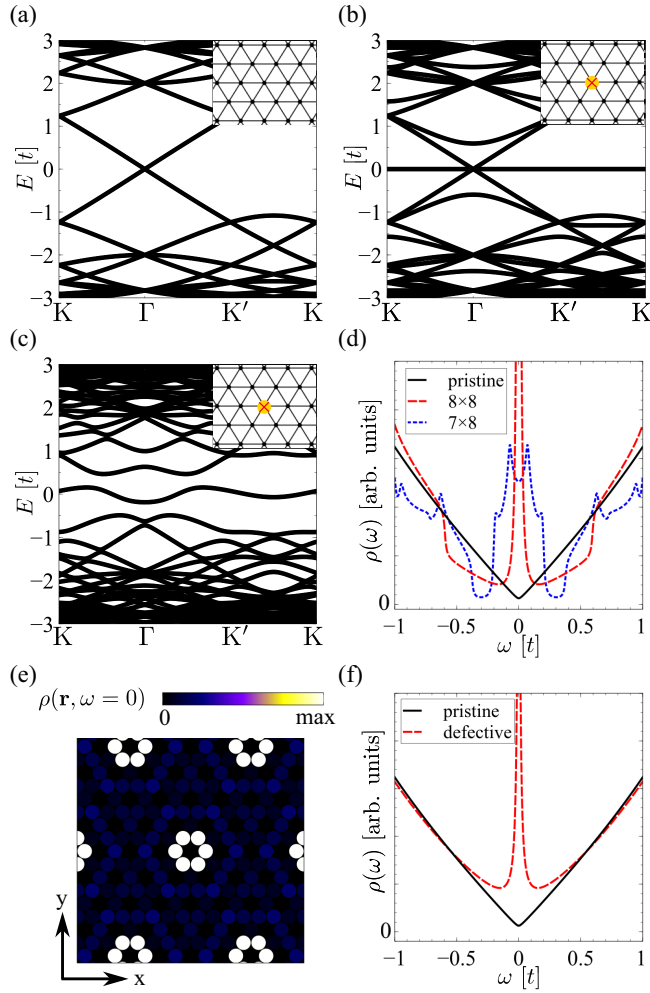
FIG. 2. Spinon excitations in pristine and defective π-flux Dirac QSL. Panel (a) shows the pristine spinon band structure of a π-flux QSL in an 8×8 unit cell. Panels (b) and (c) show the spinon band structure with a periodic array of impurities in 8×8 and 7×8 unit cells, respectively. The insets show the configurations of the impurity. Panel (d) shows the DOS corresponding to the three cases [(a)–(c)]. The divergent DOS at zero frequency corresponding to case (b) indicates the existence of zero modes, in agreement with the band structure shown in panel (b). Panel (e) shows the LDOS at zero frequency $\rho(\mathbf{r}, \omega = 0)$ for case (b). The zero modes are localized around the impurities, displaying a pattern with local C_6 rotational symmetry. Panel (f) shows the DOS of the pristine QSL and for a single impurity in an infinite QSL.

to compute the band structure and the density of states (DOS). Compared to the band structure of the pristine π-flux state, a flat band at zero energy arises for n even [Fig. 2(b)] and a wiggly band near zero energy arises for n odd [Fig. 2(c)]. In both cases, the DOS at zero frequency shows a dramatic increase [Fig. 2(d)]. The dispersive zero mode for odd n stems from the self-interaction effects of the zero mode, which are absence in the n even case. As expected, as n is increased, the zero-mode band becomes flatter even for odd n due to the decrease self-interaction between replicas. For a finite unit cell, the DOS diverges at zero frequency only when n is even, indicating the existence of resonant zero modes.

The nature of the zero mode can be analyzed by looking at the local density of states (LDOS) defined as $\rho(\mathbf{r}, \omega) = \mathrm{Im}(\langle \mathbf{r}|[\omega - H - i0^+]^{-1}|\mathbf{r}\rangle)$. In particular, the LDOS at zero frequency $\rho(\mathbf{r}, \omega = 0)$ shows that the zero modes are localized around the impurities [Fig. 2(e)], showing a pattern with local C_6 rotational symmetry. Interestingly, the zero modes are mainly localized through sites that are odd number of bonds straight away from the impurity. The previous calculation relied on assuming a periodic pattern of impurities. Experimentally, the simplest scenario will be depositing a single impurity in an infinite quantum spin liquid. In the following, we will deal with this idealized case, showing that the results are qualitatively similar to the periodic impurity pattern considered above.

C. Spinon resonances for a single impurity in an infinite Dirac spin liquid

We now move on to consider a single impurity coupled to the quantum spin liquid. In the case of a single impurity in an infinite system, translational symmetry is broken and a Bloch Hamiltonian can not be defined. To deal with this inhomogeneous infinite problem, we compute exactly the spectral function close to the impurity using a Green's function embedding method [58,79,80]. For the sake of completeness, we now summarize the essence of the method. For a unit cell containing the impurity, the Green's function in this unit cell can be written using Dyson's equation as

$$G(\omega) = [\omega - H' - \Sigma(\omega)]^{-1}, \qquad (7)$$

where H' is the Hamiltonian of the unit cell and $\Sigma(\omega)$ is the self-energy due to the coupling of the unit cell to the rest of the infinite pristine system. The impurity does not influence $\Sigma(\omega)$ since it does not change the hoppings that couple the unit cell to the rest of the system. Therefore, in the absence of the impurity, the Green's function of the pristine unit cell coupled to the infinite system is

$$G_0(\omega) = [\omega - H_0 - \Sigma(\omega)]^{-1}, \qquad (8)$$

where H_0 is the Hamiltonian of the pristine unit cell. Since the whole system is now pristine, this Green's function can also be computed by

$$G_0(\omega) = \frac{1}{(2\pi)^2} \int d^2\mathbf{k}(\omega - H_{\mathbf{k}} - i0^+)^{-1}, \qquad (9)$$

where $H_{\mathbf{k}}$ is the Bloch Hamiltonian associated to Eq. (6) on this unit cell. Using Eq. (8), the self-energy can be computed as $\Sigma(\omega) = \omega - H_0 - G_0^{-1}(\omega)$, and the Green's function of the defective unit cell can be solved with Eq. (7). The DOS is thus $\rho(\omega) = -\frac{1}{\pi}\mathrm{Im}G(\omega)$, which diverges at zero frequency for a defective unit cell [Fig. 2(f)], indicating the existence of zero modes. As a result, a single impurity in the quantum spin-liquid state also gives rise to a zero mode, as anticipated from the calculations in periodic arrays of Figs. 2(b)–2(e). We note that the embedding method presented above would allow us to compute an arbitrary cluster of impurities coupled to the quantum spin liquid, as we will address in the next section.

We have thus verified the existence of zero modes when there is (i) a periodic array of impurities with one in an $n \times m$ unit cell with n even and (ii) a single impurity in an infinite

system. This resonant zero mode stems from the vacancy boundary conditions in a Dirac system, which are known to give rise to zero modes in other Dirac systems [36]. We finally note that so far we have focused on single impurities, yet when several impurities are put together, the different zero modes are expected to give rise to interference effect. We address this interference phenomenon in the next section.

III. INTERACTION BETWEEN ZERO MODES

In this section, we investigate the interaction between zero modes by considering the case when more impurities are present. For the sake of simplicity, we first consider interference between two and three impurity sites and observe a large dependence of the net number of zero modes on their relative location. We then generalize our discussion to the thermodynamic limit when a certain density of impurities is randomly distributed, giving rise to a sublinear increase of DOS at zero frequency with respect to the impurity density due to interference effects.

A. Spinon zero mode interference between individual resonances

We first consider the case of two impurities in the Dirac quantum spin liquid, for both a periodic array and a single cluster of impurities in an otherwise pristine system Dirac QSL. In the periodic case, we consider two impurities per unit cell of size $n \times m$ with n even in order to observe interference between zero modes, as with n odd there is no zero mode in the single-vacancy case (see Sec. II). We find the relative position between the impurities strongly impacts the overall zero modes. We observe that only when the two impurities are an even number of bonds straight away from each other will there be two zero modes. In particular, we show in Fig. 3 the band structure [Figs. 3(a) and 3(b)], DOS [Figs. 3(c) and 3(d)], and LDOS [Figs. 3(e) and 3(f)] of zero modes for the cases (i) when the two impurities are two bonds away from each other [Figs. 3(a), 3(c), and 3(e)] and (ii) when the two impurities are next nearest to each other [Figs. 3(b), 3(d), and 3(f)]. For case (i), a flat band arises at zero energy in the presence of the two impurities [Fig. 3(a)], whereas in case (ii) wiggly bands at zero energy arise instead [Fig. 3(b)]. It is also interesting to note that, in the periodic case, for case (i) the dispersive bulk states remain gapless [Fig. 3(a)], whereas for case (ii) they are gapped out [Fig. 3(b)]. In both cases, the DOS at zero frequency diverges for periodic impurities and impurities in an infinite system [Figs. 3(c) and 3(d)]. The LDOS at zero frequency for both cases are similar to the summation of LDOS of zero modes for the two impurities [Figs. 3(e) and 3(f)].

The previous picture is dramatically different if the two impurities were put just next to each other, in which case no zero modes appear in the system. In this situation, the impurity states created by each impurity give rise to a bonding-antibonding splitting, lifting both the spinon resonance from zero frequency. The dependence of the existence of zero modes on the relative position between impurities can be understood by starting with the spatial of the zero-mode resonant state [Fig. 2(e)]. Let us now think in a perturbative way, in which a second vacancy can be understood as the limit
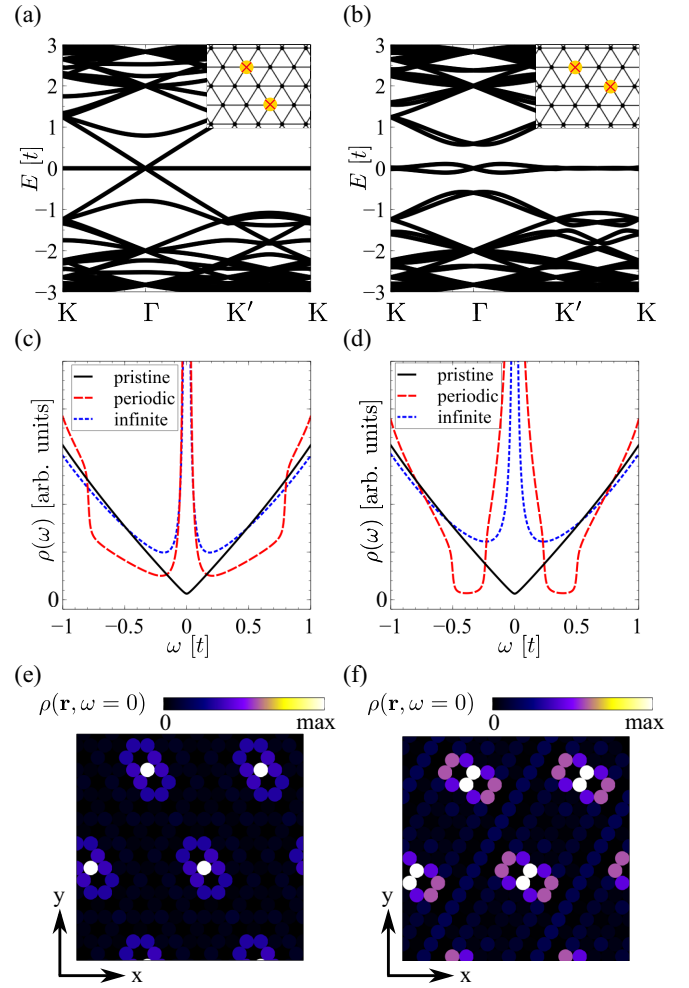

FIG. 3. Resonant zero modes with two impurities in the π-flux state. Panels (a) and (b) show the band structure of the π-flux QSL state with a periodic array of two impurities that are (a) two bonds away from each other and (b) next-nearest neighbors to each other in unit cells of size 8×8. The insets show the configurations of the impurities. Panels (c) and (d) show the DOS of the π-flux QSL state with periodic impurities and impurities in an infinite system. The impurity configurations for panels (c) and (d) are shown in panels (a) and (b), respectively. Panels (e) and (f) show the LDOS at zero frequency $\rho(\mathbf{r}, \omega = 0)$ of the π-flux state for cases (a) and (b), respectively.

where a local onsite energy is ramped up to $\pm\infty$. When an additional impurity is added to a site where the impurity zero mode is finite, perturbation theory suggests that the zero mode will be lifted from zero energy. In contrast, when the second impurity is added to a site where the LDOS at zero frequency vanishes, perturbation theory would suggest that the original mode remains at zero. We note that the previous picture is just perturbative and does not quantitatively account for the true double impurity nor the number of zero modes, but it provides a simple argument to rationalize the persistence of zero modes.

We now move on to consider the case of three impurities as shown in Fig. 4. We will focus on arrangements that still give rise to zero modes. We proceed in an analogous way,
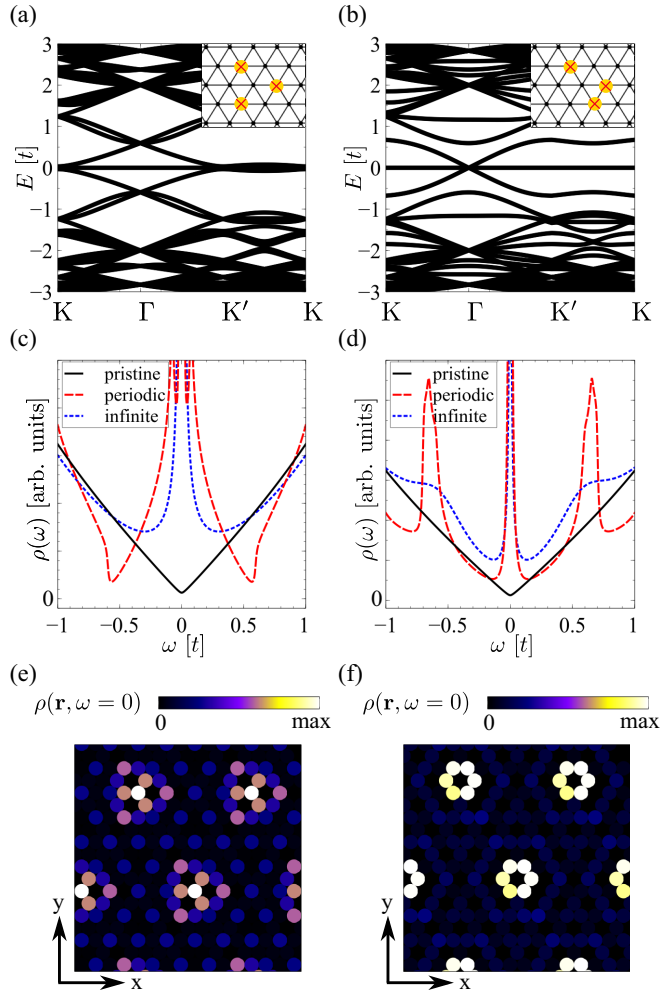
FIG. 4. Resonant zero modes with three impurities in the π-flux state. Panels (a) and (b) show the band structure of the π-flux QSL state with three impurities of different configurations shown in the insets in a unit cell of size 8×8. Panels (c) and (d) show the DOS of the π-flux QSL state with periodic impurities and impurities in an infinite system. The impurity configurations for panels (c) and (d) are shown in panels (a) and (b), respectively. Panels (e) and (f) show the LDOS at zero frequency $\rho(\mathbf{r}, \omega = 0)$ of the π-flux state for cases (a) and (b), respectively.

by showing the band structure [Figs. 4(a) and 4(b)], DOS [Figs. 4(c) and 4(d)], and LDOS [Figs. 4(e) and 4(f)]. We first focus on the case in which impurities are arranged in a C_3 symmetric fashion [Figs. 4(a), 4(c), and 4(e)], in a fashion similar to the double impurity of [Figs. 3(a), 3(c), and 3(e)]. As is shown in Fig. 4(c), a zero mode appears even with three impurities close to each other, giving rise to a zero mode with C_3 rotational symmetry. The interference of the three impurities is again highly sensitive to their relative position. In particular, by taking the limiting case of two impurities next to each other and one further apart [Figs. 4(b) and 4(d) 4(f)], we observe a zero-frequency peak surrounded by two peaks at positive and negative frequencies [Fig. 4(d)]. The two peaks above and below zero can be understood as the bonding and antibonding impurity resonances associated to the closest impurities, whereas the remaining zero-frequency peak will

be be associated to the remaining impurity. This is also shown in Fig. 4(f), where it can be seen that the zero mode is located around the remaining impurity, with a small C_6 symmetry breaking induced by the other two impurities. These results highlight that the interaction between zero modes created by different impurities will give rise to nontrivial interference effects. In particular, this will give rise to a density of zero modes sublinear with the impurity density as we address below.

B. Thermodynamic limit and zero mode quenching

We now address the emergence of zero modes in a disordered system with a varying number of impurities. In particular, we will show how the interference of zero modes can be observed by tracking the spinon DOS near zero frequency for different impurity densities. We start by discussing an idealized case in which there are no interference effect. If there were no interactions between different zero modes, the density of zero modes should increase linearly with respect to the impurity density, assuming that each new impurity would create a new zero mode. In this idealized case, the expected density of states $\rho_0(\nu, \omega)$ at a certain impurity density ν would fulfill

$$\lim_{\omega \to 0} \rho_0(\nu, \omega) = \lim_{\omega \to 0} \left(\rho(0, \omega) + \frac{\nu}{\nu_0} \rho(\nu = \nu_0, \omega) \right) \quad (10)$$

with ω near 0, ν_0 being a small finite impurity concentration, and $\rho(\nu, \omega)$ being the true density of states of the system computed exactly. In the following, we take $\nu_0 = 0.01$, and we verify that our results remain qualitatively similar with other small values. We now compute the density of states $\rho(\nu, \omega)$ for different impurity densities and at different energy using the kernel polynomial method (KPM) [81] and averaging over impurity distributions. We consider random impurity distributions with densities ν from 0.01 to 0.3, where $\nu = 1$ would mean vacancies in every site. We take a unit cell of size 50×50 and show $\rho(\nu, \omega)/\rho_0(\nu, \omega)$, the ratio of the computed exact DOS over the expected DOS in the absence of interference, for different ν and ω (Fig. 5).

In the ideal case in which impurity interferences are negligible, the ratio $\rho(\nu, \omega)/\rho_0(\nu, \omega)$ would be one for $\omega \to 0$, as is observed at small ν in Fig. 5(a). This is easily rationalized by taking into account that at small concentrations, interference effects between impurities are statistically unlikely, and therefore the system behaves as if each impurity is isolated. This is also seen by inspecting the disorder average DOS for $\nu = 0.01$ as shown in Fig. 5(b), which resembles the result obtained for a single impurity in an infinite system shown in Fig. 2(d). This situation dramatically changes as the impurity concentration increases, as can be observed for large values of ν in Fig. 5(a). In particular, it is shown in Fig. 5(c) the DOS for $\nu = 0.25$, highlighting that the zero-mode peak has become less sharp in comparison with the bulk states.

It is finally worth noting that for larger impurity concentrations, the spinon ground state may suffer a reconstruction in a real experiment and lose its Dirac nature, and therefore impurity interference effects are better experimentally explored at low impurity densities. This brings up the question on how such zero-energy resonances in the spinon spectra can
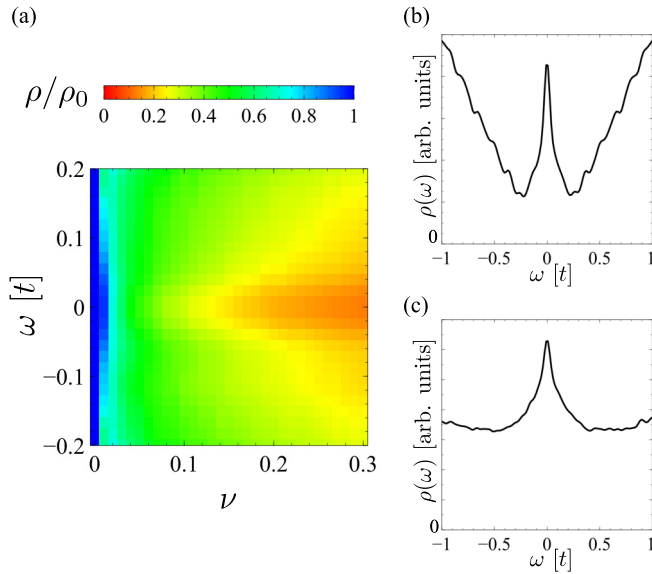
FIG. 5. (a) Ratio of the computed DOS over the expected DOS in the absence of interference effects $\rho(\nu, \omega)/\rho_0(\nu, \omega)$ for different impurity density ν in the π-flux state. The sublinear increase of such ratio with respect to ν at $\omega = 0$ indicates the existence of interference effects between different zero modes. Panel (b) shows the DOS for the π-flux state at impurity density $\nu = 0.01$, a low impurity concentration showing negligible interference. Panel (c) shows the DOS for the π-flux state at impurity density $\nu = 0.25$, showing a broader peak stemming from the interference and quenching between vacancy states.

be experimentally detected, which is addressed in the next section.

IV. EXPERIMENTAL DETECTION OF SPINON ZERO MODES

We now consider the potential experimental signatures of these spinon zero modes. In particular, scanning tunnel spectroscopic techniques have been demonstrated to be very well suited to detect quantum spin excitations [74], as demonstrated in a variety of experiments showing atomic-scale magnons [82], quantum critical transitions [83], and quantum transitions in nanomagnets [72]. In particular, two different techniques can be used to probe magnetic excitations with scanning tunnel microscopy (STM): Inelastic spectroscopy [61,70,84] and electrically driven paramagnetic resonance [85–94]. Inelastic resonance experiments rely on measuring current versus voltage between the tip and the sample and identifying steps in the differential conductance dI/dV. These steps are associated with inelastic processes in which an electron tunnels creating an excitation, namely a phonon [95] or spin excitation [82]. In particular, neglecting phonon contributions at small biases, inelastic steps will appear as peaks in the d^2I/dV^2 and are proportional to the spectral function of spin excitations [82]

$$d^2I/dV^2 \sim \langle\Omega|S_i^+\delta(\omega - \mathcal{H} + E_\Omega)S_i^-|\Omega\rangle \qquad (11)$$
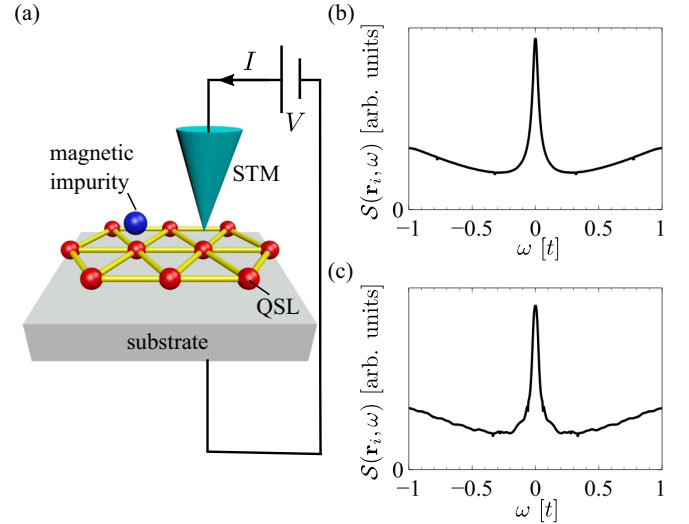

FIG. 6. (a) Sketch of the experimental setup to measure the resonant Dirac spinons close to the impurity by means of inelastic spectroscopy or electrically driven paramagnetic resonance. Panels (b) and (c) show the local spin structure factor $\mathcal{S}(\mathbf{r}_i, \omega)$, computed on the site near the impurity: (b) a single impurity in an infinite system and (c) a single impurity in a large finite system (with 100×100 sites). It is observed that a zero-bias peak appears, which is associated with the original divergent spinon density of states at zero frequency.

where $|\Omega\rangle$ is the many-body ground state and E_Ω is the many-body ground-state energy. The quantity in Eq. (11) is proportional to the so-called spin structure factor $\mathcal{S}(\mathbf{r}_i, \omega)$, which can be understood as the magnon density of states in a ferromagnet, or the $\Delta S = 1$ excitations in a generic spin system. In the particular case of a quantum spin-liquid state, $\Delta S = 1$ involves creating two-spinon excitations, and as a result provides information about the two-spinon spectral function. Furthermore, besides inelastic spectroscopy, the spin structure factor can be accessed by electrically driven paramagnetic resonance with STM [91]. This technique has been further demonstrated to allow for measuring spin excitations with a resolution not limited by temperature [85,91,92], turning it into a well-suited technique to probe the low-energy scales expected in quantum spin-liquid systems.

In the partonic spinon language, the spin structure factor will be proportional to the density-density response function of the spinons. We will compare our results between a single impurity coupled to an infinite and otherwise pristine QSL computed with the embedding method [Fig. 6(b)] and a single impurity in a finite large system computed with the KPM [81] [Fig. 6(c)]. It is important to note that, in the following and for the sake of simplicity, we will be neglecting gauge fluctuations. Within this approximation, the spin structure factor becomes $\mathcal{S}(\mathbf{r}_i, \omega) \sim \sum_{n,n'} \frac{f_n - f_{n'}}{\omega + \varepsilon_n - \varepsilon_{n'} + i\eta} \psi_n^*(\mathbf{r}_i)\psi_{n'}(\mathbf{r}_i)\psi_n(\mathbf{r}_i)\psi_{n'}^*(\mathbf{r}_i)$, where ψ_n is the nth spinon eigenstates with energy ε_n, and f_n is the Fermi-Dirac distribution. It is now convenient to rewrite $\mathcal{S}(\mathbf{r}_i, \omega)$ in terms of the local spectral function $\rho(\mathbf{r}_i, \mathbf{r}_i, \omega) =$

$\sum_n \psi_n^*(\mathbf{r}_i)\psi_n(\mathbf{r}_i)\delta(\omega - E_n)$, so that the spin structure factor becomes

$$\mathcal{S}(\mathbf{r}_i, \omega) \sim \int d\omega_1 d\omega_2 \frac{\rho(\mathbf{r}_i, \mathbf{r}_i, \omega_1)\rho(\mathbf{r}_i, \mathbf{r}_i, \omega_2)}{\omega + \omega_1 - \omega_2 + i\eta}$$
$$\times [f(\omega_1) - f(\omega_2)]. \tag{12}$$

The local spin structure factor is computed for the site near the impurity [Fig. 6(b)], where the Green's function is computed using the embedding method introduced in Sec. II. Alternatively, we also show the spin structure factor computed for a finite quantum spin-liquid system with 10 000 sites [Fig. 6(c)] using the KPM [81]. In both instances, it is observed a zero-bias peak, which is associated to the divergent density of states of the spinon excitations.

The previous result highlights that the spinon zero-mode resonances will appear as a divergent peak at small biases. In a similar fashion, the different arrangements between magnetic impurities will give rise to spectra resembling a self-convolution of the spinon density of states. This feature may allow us to distinguish Dirac spin-liquid states from another generic kind of magnetically ordered state, as resonant-like zero-bias peak for $S = 1/2$ will not appear for a generically coupled magnetic state. We finally note that the previous picture relies on assuming that the tunneling signal stems solely from spin-flip processes, and neglects orbital or Kondo-like transitions that can be present in the real setup.

V. CONCLUSION

We have shown that individual magnetic $S = 1/2$ impurities coupled to a Dirac quantum spin-liquid state, as realized in NaYbO$_2$, give rise to a divergent spinon density of states at zero frequency. The emergence of such zero modes is associated with the low-energy Dirac nature of the spinon excitations and as a result provides a simple spectroscopic signature distinguishing Dirac spin liquids from generic gapless Dirac liquids with a finite Fermi surface. We have shown that such spinon zero modes give rise to a zero frequency divergence in the spin structure factor that can be measured by means of inelastic spectroscopy and electrically driven paramagnetic resonance with scanning tunnel microscopy. Interestingly, although the emergence of zero-bias peaks in inelastic spectroscopy due to a magnetic impurity is commonly associated with Kondo physics, the phenomena presented relies on single-particle spinon physics and it is therefore not related with a spinon-induced Kondo state. Our results put forward impurity engineering by scanning probe techniques as a simple method to probe quantum spin-liquid physics by a local real space measurement.

[1] P. A. Lee, Science **321**, 1306 (2008).

[2] L. Balents, Nature (London) **464**, 199 (2010).

[3] J. G. Rau, E. K.-H. Lee, and H.-Y. Kee, Annu. Rev. Condens. Matter Phys. **7**, 195 (2016).

[4] S. H. Chun, J.-W. Kim, J. Kim, H. Zheng, C. C. Stoumpos, C. D. Malliakas, J. F. Mitchell, K. Mehlawat, Y. Singh, Y. Choi, T. Gog, A. Al-Zein, M. M. Sala, M. Krisch, J. Chaloupka, G. Jackeli, G. Khaliullin, and B. J. Kim, Nat. Phys. **11**, 462 (2015).

[5] P. Anderson, Mater. Res. Bull. **8**, 153 (1973).

[6] C. Broholm, R. J. Cava, S. A. Kivelson, D. G. Nocera, M. R. Norman, and T. Senthil, Science **367**, eaay0668 (2020).

[7] Y. Zhou, K. Kanoda, and T.-K. Ng, Rev. Mod. Phys. **89**, 025003 (2017).

[8] L. Savary and L. Balents, Rep. Prog. Phys. **80**, 016502 (2016).

[9] A. Kitaev, Ann. Phys. **321**, 2 (2006).

[10] P. W. Anderson, Science **235**, 1196 (1987).

[11] Z. A. Kelly, M. J. Gallagher, and T. M. McQueen, Phys. Rev. X **6**, 041007 (2016).

[12] T.-H. Han, J. S. Helton, S. Chu, D. G. Nocera, J. A. Rodriguez-Rivera, C. Broholm, and Y. S. Lee, Nature (London) **492**, 406 (2012).

[13] M. Fu, T. Imai, T.-H. Han, and Y. S. Lee, Science **350**, 655 (2015).

[14] B. J. Powell and R. H. McKenzie, Rep. Prog. Phys. **74**, 056501 (2011).

[15] S. K. Takahashi, J. Wang, A. Arsenault, T. Imai, M. Abramchuk, F. Tafti, and P. M. Singer, Phys. Rev. X **9**, 031047 (2019).

[16] M. R. Norman, Rev. Mod. Phys. **88**, 041002 (2016).

[17] H. Takagi, T. Takayama, G. Jackeli, G. Khaliullin, and S. E. Nagler, Nat. Rev. Phys. **1**, 264 (2019).

[18] Y. Shimizu, K. Miyagawa, K. Kanoda, M. Maesato, and G. Saito, Phys. Rev. Lett. **91**, 107001 (2003).

[19] M. Yamashita, N. Nakata, Y. Kasahara, T. Sasaki, N. Yoneyama, N. Kobayashi, S. Fujimoto, T. Shibauchi, and Y. Matsuda, Nat. Phys. **5**, 44 (2009).

[20] T. Itou, A. Oyamada, S. Maegawa, M. Tamura, and R. Kato, Phys. Rev. B **77**, 104413 (2008).

[21] T. Isono, H. Kamo, A. Ueda, K. Takahashi, M. Kimata, H. Tajima, S. Tsuchiya, T. Terashima, S. Uji, and H. Mori, Phys. Rev. Lett. **112**, 177201 (2014).

[22] J. S. Helton, K. Matan, M. P. Shores, E. A. Nytko, B. M. Bartlett, Y. Yoshida, Y. Takano, A. Suslov, Y. Qiu, J.-H. Chung, D. G. Nocera, and Y. S. Lee, Phys. Rev. Lett. **98**, 107204 (2007).

[23] L. Ding, P. Manuel, S. Bachus, F. Grußler, P. Gegenwart, J. Singleton, R. D. Johnson, H. C. Walker, D. T. Adroja, A. D. Hillier, and A. A. Tsirlin, Phys. Rev. B **100**, 144432 (2019).

[24] M. M. Bordelon, E. Kenney, C. Liu, T. Hogan, L. Posthuma, M. Kavand, Y. Lyu, M. Sherwin, N. P. Butch, C. Brown, M. J. Graf, L. Balents, and S. D. Wilson, Nat. Phys. **15**, 1058 (2019).

[25] K. T. Law and P. A. Lee, Proc. Natl. Acad. Sci. USA **114**, 6996 (2017).

[26] M. Klanjšek, A. Zorko, R. Žitko, J. Mravlje, Z. Jagličić, P. K. Biswas, P. Prelovšek, D. Mihailovic, and D. Arčon, Nat. Phys. **13**, 1130 (2017).

[27] Y. Chen, W. Ruan, M. Wu, S. Tang, H. Ryu, H.-Z. Tsai, R. Lee, S. Kahn, F. Liou, C. Jia, O. R. Albertini, H. Xiong, T. Jia, Z. Liu,

J. A. Sobota, A. Y. Liu, J. E. Moore, Z.-X. Shen, S. G. Louie, S.-K. Mo, and M. F. Crommie, Nat. Phys. **16**, 218 (2020).

[28] A. Banerjee, C. A. Bridges, J.-Q. Yan, A. A. Aczel, L. Li, M. B. Stone, G. E. Granroth, M. D. Lumsden, Y. Yiu, J. Knolle, S. Bhattacharjee, D. L. Kovrizhin, R. Moessner, D. A. Tennant, D. G. Mandrus, and S. E. Nagler, Nat. Mater. **15**, 733 (2016).

[29] F. de Juan, J. L. Mañes, and M. A. H. Vozmediano, Phys. Rev. B **87**, 165131 (2013).

[30] F. Guinea, M. I. Katsnelson, and A. K. Geim, Nat. Phys. **6**, 30 (2009).

[31] N. Levy, S. A. Burke, K. L. Meaker, M. Panlasigui, A. Zettl, F. Guinea, A. H. C. Neto, and M. F. Crommie, Science **329**, 544 (2010).

[32] E. Suárez Morell, J. D. Correa, P. Vargas, M. Pacheco, and Z. Barticevic, Phys. Rev. B **82**, 121407(R) (2010).

[33] R. Bistritzer and A. H. MacDonald, Proc. Natl. Acad. Sci. USA **108**, 12233 (2011).

[34] Y. Cao, V. Fatemi, S. Fang, K. Watanabe, T. Taniguchi, E. Kaxiras, and P. Jarillo-Herrero, Nature (London) **556**, 43 (2018).

[35] Y. Cao, V. Fatemi, A. Demir, S. Fang, S. L. Tomarken, J. Y. Luo, J. D. Sanchez-Yamagishi, K. Watanabe, T. Taniguchi, E. Kaxiras, R. C. Ashoori, and P. Jarillo-Herrero, Nature (London) **556**, 80 (2018).

[36] V. M. Pereira, F. Guinea, J. M. B. Lopes dos Santos, N. M. R. Peres, and A. H. Castro Neto, Phys. Rev. Lett. **96**, 036801 (2006).

[37] H. Gonzalez-Herrero, J. M. Gomez-Rodriguez, P. Mallet, M. Moaied, J. J. Palacios, C. Salgado, M. M. Ugeda, J.-Y. Veuillen, F. Yndurain, and I. Brihuega, Science **352**, 437 (2016).

[38] H. Alloul, J. Bobroff, M. Gabay, and P. J. Hirschfeld, Rev. Mod. Phys. **81**, 45 (2009).

[39] A. P. Mackenzie and Y. Maeno, Rev. Mod. Phys. **75**, 657 (2003).

[40] R. Balian and N. R. Werthamer, Phys. Rev. **131**, 1553 (1963).

[41] D. F. Agterberg, Phys. Rev. B **60**, R749(R) (1999).

[42] K. Maki and S. Haas, Phys. Rev. B **62**, R11969(R) (2000).

[43] B. Zinkl, M. H. Fischer, and M. Sigrist, Phys. Rev. B **100**, 014519 (2019).

[44] P. Anderson, J. Phys. Chem. Solids **11**, 26 (1959).

[45] A. V. Balatsky, I. Vekhter, and J.-X. Zhu, Rev. Mod. Phys. **78**, 373 (2006).

[46] H. Shiba, Prog. Theor. Phys. **40**, 435 (1968).

[47] A. I. Rusinov, Sov. J. Exp. Theor. Phys. Lett. **9**, 85 (1969).

[48] P. T. Sprunger, L. Petersen, E. W. Plummer, E. Lægsgaard, and F. Besenbacher, Science **275**, 1764 (1997).

[49] L. Petersen, P. T. Sprunger, P. Hofmann, E. Lægsgaard, B. G. Briner, M. Doering, H.-P. Rust, A. M. Bradshaw, F. Besenbacher, and E. W. Plummer, Phys. Rev. B **57**, R6858(R) (1998).

[50] A. Weismann, M. Wenderoth, S. Lounis, P. Zahn, N. Quaas, R. G. Ulbrich, P. H. Dederichs, and S. Blugel, Science **323**, 1190 (2009).

[51] E. J. Duplock, M. Scheffler, and P. J. D. Lindan, Phys. Rev. Lett. **92**, 225502 (2004).

[52] O. V. Yazyev, Rep. Prog. Phys. **73**, 056501 (2010).

[53] O. V. Yazyev and L. Helm, Phys. Rev. B **75**, 125408 (2007).

[54] J. J. Palacios, J. Fernández-Rossier, and L. Brey, Phys. Rev. B **77**, 195428 (2008).

[55] P. O. Lehtinen, A. S. Foster, Y. Ma, A. V. Krasheninnikov, and R. M. Nieminen, Phys. Rev. Lett. **93**, 187202 (2004).

[56] A. Lopez-Bezanilla and J. L. Lado, Phys. Rev. Mater. **3**, 084003 (2019).

[57] D. W. Boukhvalov, M. I. Katsnelson, and A. I. Lichtenstein, Phys. Rev. B **77**, 035427 (2008).

[58] N. A. García-Martínez, J. L. Lado, D. Jacob, and J. Fernández-Rossier, Phys. Rev. B **96**, 024403 (2017).

[59] C. F. Hirjibehedin, C.-Y. Lin, A. F. Otte, M. Ternes, C. P. Lutz, B. A. Jones, and A. J. Heinrich, Science **317**, 1199 (2007).

[60] A. F. Otte, M. Ternes, K. von Bergmann, S. Loth, H. Brune, C. P. Lutz, C. F. Hirjibehedin, and A. J. Heinrich, Nat. Phys. **4**, 847 (2008).

[61] S. Loth, K. von Bergmann, M. Ternes, A. F. Otte, C. P. Lutz, and A. J. Heinrich, Nat. Phys. **6**, 340 (2010).

[62] A. F. Otte, M. Ternes, S. Loth, C. P. Lutz, C. F. Hirjibehedin, and A. J. Heinrich, Phys. Rev. Lett. **103**, 107203 (2009).

[63] S. Loth, S. Baumann, C. P. Lutz, D. M. Eigler, and A. J. Heinrich, Science **335**, 196 (2012).

[64] C. F. Hirjibehedin, C. P. Lutz, and A. J. Heinrich, Science **312**, 1021 (2006).

[65] E. Liebhaber, S. A. González, R. Baba, G. Reecht, B. W. Heinrich, S. Rohlf, K. Rossnagel, F. von Oppen, and K. J. Franke, Nano Lett. **20**, 339 (2019).

[66] L. Farinacci, G. Ahmadi, G. Reecht, M. Ruby, N. Bogdanoff, O. Peters, B. W. Heinrich, F. von Oppen, and K. J. Franke, Phys. Rev. Lett. **121**, 196803 (2018).

[67] S. Kezilebieke, R. Žitko, M. Dvorak, T. Ojanen, and P. Liljeroth, Nano Lett. **19**, 4614 (2019).

[68] L. Gross, F. Mohn, P. Liljeroth, J. Repp, F. J. Giessibl, and G. Meyer, Science **324**, 1428 (2009).

[69] R. Drost, T. Ojanen, A. Harju, and P. Liljeroth, Nat. Phys. **13**, 668 (2017).

[70] A. J. Heinrich, J. A. Gupta, C. P. Lutz, and D. M. Eigler, Science **306**, 466 (2004).

[71] M. Ternes, C. P. Lutz, C. F. Hirjibehedin, F. J. Giessibl, and A. J. Heinrich, Science **319**, 1066 (2008).

[72] K. Yang, Y. Bae, W. Paul, F. D. Natterer, P. Willke, J. L. Lado, A. Ferrón, T. Choi, J. Fernández-Rossier, A. J. Heinrich, and C. P. Lutz, Phys. Rev. Lett. **119**, 227206 (2017).

[73] F. E. Kalff, M. P. Rebergen, E. Fahrenfort, J. Girovsky, R. Toskovic, J. L. Lado, J. Fernández-Rossier, and A. F. Otte, Nat. Nanotechnol. **11**, 926 (2016).

[74] D.-J. Choi, N. Lorente, J. Wiebe, K. von Bergmann, A. F. Otte, and A. J. Heinrich, Rev. Mod. Phys. **91**, 041001 (2019).

[75] S. Hu, W. Zhu, S. Eggert, and Y.-C. He, Phys. Rev. Lett. **123**, 207203 (2019).

[76] J. Iaconis, C. Liu, G. B. Halász, and L. Balents, SciPost Phys. **4**, 003 (2018).

[77] Z. Zhu, P. A. Maksimov, S. R. White, and A. L. Chernyshev, Phys. Rev. Lett. **120**, 207203 (2018).

[78] Y. Iqbal, W.-J. Hu, R. Thomale, D. Poilblanc, and F. Becca, Phys. Rev. B **93**, 144411 (2016).

[79] D. Jacob and G. Kotliar, Phys. Rev. B **82**, 085423 (2010).

[80] J. L. Lado and J. Fernández-Rossier, 2D Mater. **3**, 025001 (2016).

[81] A. Weiße, G. Wellein, A. Alvermann, and H. Fehske, Rev. Mod. Phys. **78**, 275 (2006).

[82] A. Spinelli, B. Bryant, F. Delgado, J. Fernández-Rossier, and A. F. Otte, Nat. Mater. **13**, 782 (2014).

[83] R. Toskovic, R. van den Berg, A. Spinelli, I. S. Eliens, B. van den Toorn, B. Bryant, J.-S. Caux, and A. F. Otte, Nat. Phys. **12**, 656 (2016).

[84] J. Fernández-Rossier, Phys. Rev. Lett. **102**, 256802 (2009).

[85] F. D. Natterer, K. Yang, W. Paul, P. Willke, T. Choi, T. Greber, A. J. Heinrich, and C. P. Lutz, Nature (London) **543**, 226 (2017).

[86] Y. Bae, K. Yang, P. Willke, T. Choi, A. J. Heinrich, and C. P. Lutz, Sci. Adv. **4**, eaau4159 (2018).

[87] P. Willke, W. Paul, F. D. Natterer, K. Yang, Y. Bae, T. Choi, J. Fernández-Rossier, A. J. Heinrich, and C. P. Lutz, Sci. Adv. **4**, eaaq1543 (2018).

[88] P. Willke, K. Yang, Y. Bae, A. J. Heinrich, and C. P. Lutz, Nat. Phys. **15**, 1005 (2019).

[89] P. Willke, A. Singha, X. Zhang, T. Esat, C. P. Lutz, A. J. Heinrich, and T. Choi, Nano Lett. **19**, 8201 (2019).

[90] T. S. Seifert, S. Kovarik, C. Nistor, L. Persichetti, S. Stepanow, and P. Gambardella, Phys. Rev. Res. **2**, 013032 (2020).

[91] S. Baumann, W. Paul, T. Choi, C. P. Lutz, A. Ardavan, and A. J. Heinrich, Science **350**, 417 (2015).

[92] P. Willke, Y. Bae, K. Yang, J. L. Lado, A. Ferrón, T. Choi, A. Ardavan, J. Fernández-Rossier, A. J. Heinrich, and C. P. Lutz, Science **362**, 336 (2018).

[93] J. L. Lado, A. Ferrón, and J. Fernández-Rossier, Phys. Rev. B **96**, 205420 (2017).

[94] A. Ferrón, S. A. Rodríguez, S. S. Gómez, J. L. Lado, and J. Fernández-Rossier, Phys. Rev. Res. **1**, 033185 (2019).

[95] L. Vitali, M. A. Schneider, K. Kern, L. Wirtz, and A. Rubio, Phys. Rev. B **69**, 121414(R) (2004).